Nondiffusive decay of gradient-driven fluctuations in a free-diffusion process

Fabrizio Croccolo,[1,*] Doriano Brogioli,[1,†] Alberto Vailati,[1] Marzio Giglio,[1] and David S. Cannell[2]
[1]*CNR-INFM and Dipartimento di Fisica, Università degli Studi di Milano, Via Celoria 16, Milano 20133, Italy*
[2]*Department of Physics and iQCD, University of California at Santa Barbara, Santa Barbara, California 93106, USA*
(Received 8 April 2007; published 5 October 2007)

We report the results of an experimental study of the static and dynamic properties of long wavelength concentration fluctuations in a mixture of glycerol and water undergoing free diffusion. The shadowgraph method was used to measure both the mean-squared amplitude and the temporal correlation function of the fluctuations for wave vectors so small as to be inaccessible to dynamic light scattering. For a fluid with a stabilizing vertical concentration gradient, the fluctuations are predicted to have a decay rate that *increases* with decreasing wave vector q, for wave vectors below a cutoff wave vector q_C, determined by gravity and the fluid properties. This behavior is caused by buoyant forces acting on the fluctuations. We find that for wave vectors above $\sim q_C$, the decay rate does vary in the normal diffusive manner as Dq^2, where D is the mass diffusion coefficient. Furthermore, for $q \lesssim q_C$ we find that longer wavelength fluctuations decay more *rapidly* than do shorter wavelength fluctuations, i.e., the behavior is nondiffusive, as predicted.

DOI: 10.1103/PhysRevE.76.041112 PACS number(s): 05.40.−a, 68.05.−n, 47.90.+a

I. INTRODUCTION

It is well established that single-component fluids subjected to stabilizing temperature gradients develop spatially long-ranged fluctuations whose mean-squared amplitude increases with decreasing wave vector [1–21]. As a reflection of this behavior, the structure factor $S(q,\omega)$ describing the spatial and temporal behavior of fluctuations in fluids is severely modified by the presence of a gradient. The effect is most pronounced for fluctuations having wave vectors q, lying in a plane perpendicular to the gradient. For a bulk sample in the absence of gravity, the mean-squared amplitude of such fluctuations is predicted to diverge as q^{-4}, rather than to be q independent for small q, as it is for a fluid in equilibrium. This effect was predicted by Kirkpatrick, Cohen, and Dorfman in 1982, using mode coupling and kinetic theory [6–8]. Their initial calculations did not include the effects of gravity or boundaries; however this was soon rectified [11,12]. It was also realized that the same results could be obtained more easily [9] using Landau's theory of fluctuating hydrodynamics [22]. This approach has allowed the incorporation of both gravitational and boundary effects [12,17–21,23] into the calculations, and has allowed such realistic calculations to be extended to binary mixtures as well [23–28]. Very recently a monograph has appeared on the subject [29].

The effect of gravity on an unbounded single-component fluid with a linear stabilizing vertical temperature gradient [17], or upon an unbounded mixture with a linear stabilizing vertical concentration gradient [24,25], is to introduce a gravitational cutoff, resulting in a static structure factor (mean-squared fluctuation amplitude) that varies as $[1+(q/q_C)^4]^{-1}$. The cutoff wave vector q_C, is given by $q_C = [\alpha g \nabla T/(\nu D_T)]^{1/4}$, for a single-component fluid and by $q_C = [\beta g \nabla c/(\nu D)]^{1/4}$ for a mixture. Here α and β are the thermal and solutal expansion coefficients, respectively, c is the concentration, ν is the kinematic viscosity, and D_T and D are the thermal and mass diffusivities, respectively. Physically, velocity fluctuations couple to the thermal and/or concentration fluctuations, and this coupling results in large amplitude, long wavelength fluctuations in the temperature and/or concentration. These fluctuations are predicted to be quenched by gravitational forces for sufficiently small q, resulting in a crossover from q^{-4} behavior to q-independent behavior at small q, in the absence of boundaries.

An attempt to extend the theory to fluid mixtures undergoing free diffusion has been made [25]. In this case, no thermal gradient is present, but the concentration gradient, and in principle the fluid properties, are dependent upon both vertical position z, and time t, as the concentration profile evolves. The predictions are very similar to those for fluids with linear gradients, except that q_C and $S(q,\omega)$ are dependent on both z and t.

The q^{-4} divergence in $S(q)$ has been studied experimentally for single-component fluids [13,15,16,30] and for mixtures [25,30–35], both with linear stabilizing gradients, usually for wave vectors well above q_C. Ultra-low-angle light scattering, and/or shadowgraph methods have been used to measure $S(q)$ [25,36–40] for several mixtures undergoing free diffusion during the dissolution of an initially sharp interface, and during the transient period [33] after application of a temperature gradient to a mixture near its consolute critical point, where the Soret effect is remarkably strong. In several studies, both the q^{-4} divergence and the development of a gravitational cutoff are evident in the data [25,32,34,36].

The effect of a gradient on the dynamics of the fluctuations is also predicted to be dramatic. For a single-component fluid or a mixture, both with a linear stabilizing gradient, the primary effect is to convert the normally independent viscous and either thermal or concentration modes

*Present address: Dipartimento di Fisica "G. Occhialini" and PLASMAPROMETEO, Università degli Studi di Milano-Bicocca, Piazza della Scienza 3, Milano 20126, Italy.
†Present address: Dipartimento di Fisica "G. Occhialini" and INFN, Università degli Studi di Milano-Bicocca, Piazza della Scienza 3, Milano 20126, Italy.

into a pair of coupled modes. These coupled modes are predicted to behave diffusively, i.e., to have a decay rate proportional to q^2, for q well above q_C [17,24], and this regime has been studied in mixtures using dynamic light scattering [13,15,30]. The fluctuations are predicted [12,41,42] to become propagating for sufficiently small q, both in mixtures and single-component fluids. This effect has been observed for a single-component fluid with a stabilizing gradient, using a forced scattering technique [42].

The dynamics of fluctuations while heating from below (destabilizing gradient) have been studied by Oh *et al.* [43], using a shadowgraph, in a very thin layer (34.3 μm) of near critical SF_6, below the onset of convection. By measuring the reduction in $S(q)$ caused by increasing exposure time, they were able to deduce the decay rates of fluctuations, assuming the decay to be exponential. (Increasing exposure time averages out the fluctuations to an extent dependent on the decay rate.) They observed nondiffusive behavior for the decay rate, which reached a minimum near the wave vector at which convection rolls formed just above the onset of convection, and then *increased* with *decreasing* wave vector, much as we observe. Unlike the free-diffusion case we have studied, gravity plays little role under the conditions of their experiment; instead, the nondiffusive behavior is caused primarily by the proximity of conducting boundaries that essentially "short-circuit" long wavelength temperature fluctuations, and cause them to decay much more rapidly than they would in bulk fluid.

A theoretically challenging situation also prevails during free-diffusion processes, as mentioned above. To our knowledge, this situation has been treated theoretically only in [25], and in order to make contact with experiment, they were forced to make the strong simplifying assumption that the fluctuations are uncorrelated in the z direction. For the case of mixtures, both with linear stabilizing gradients [24] and while undergoing free diffusion [25], theories predict a very interesting effect, which might be termed nondiffusive behavior. For wave vectors well above q_C, the spectral linewidth (decay rate), is predicted to behave normally, i.e., as Dq^2, while below q_C, but for wave vectors sufficiently large that the fluctuations do not propagate, the decay rate is predicted to crossover to q^{-2} behavior. That is to say, longer wavelength fluctuations are predicted to decay *more rapidly* than do shorter wavelength fluctuations in this intermediate regime. Thus, the decay rate Γ, should have a minimum near q_C and actually rise at small q. Specifically, Γ is predicted to be well approximated by $\Gamma = Dq^2[1+(q_C/q)^4]$, under the appropriate conditions [25]. This nondiffusive behavior (not to be confused with nonexponential decay of the correlation function) is a direct manifestation of the effect of gravity on the dynamics of long wavelength fluctuations in a mixture with a stabilizing gradient. For free diffusion, with significant z dependence of the gradient and/or fluid properties, Γ will however, be z dependent.

In this paper, we report the results of an experimental investigation of the dynamics of fluctuations in a mixture undergoing free diffusion. Our results pertain to the intermediate-q regime, where the fluctuations behave nondiffusively but do not propagate, as they are predicted to do for sufficiently small q. We have observed the predicted crossover from the q^2 behavior of the decay rate at higher q, and clearly observe a minimum in the decay rate vs q. The experiments were carried out by injecting a mixture consisting of 39% glycerol by weight in water beneath a layer of water, and using the shadowgraph method to measure the correlation function [Fourier transform of $S(q,\omega)$ with respect to ω] of the fluctuations for wave vectors ranging from about 50 cm^{-1} to over 500 cm^{-1}. Use of the shadowgraph method allowed us to access such small wave vectors, which are inaccessible by even small-angle light scattering because of stray elastically scattered light. In addition to the nondiffusive behavior of the decay rate described above, we also observed the correlation functions to decay exponentially at sufficiently high q, and to exhibit nonexponential decay for sufficiently small wave vector. We find that the decay rate (as measured by the inverse of the time required for the correlation functions to decay to e^{-1} of their initial values) reaches a minimum near the critical wave vector, as predicted. The remainder of this paper consists of three sections. Section II describes the experimental methods, Sec. III presents the results and analysis, and Sec. IV provides a brief discussion.

II. EXPERIMENTAL METHODS

The sample was confined within a cylindrical glass cell (Hellma model 120-OS-20), 20 mm in inner diameter with plane parallel windows 2.0 cm apart fused to its ends. The cell windows were oriented horizontally. A silicone rubber stopper on the side of the cell was fitted with two syringe needles, one of which ended near the bottom of the cell, and the other of which ended somewhat above the midplane. This arrangement allowed the cell to be completely filled initially with one fluid simply by inverting it while filling, and then to inject a second, denser fluid, in a horizontal layer beneath the first. The cell was originally filled with degassed water, and the denser glycerol/water mixture was carefully injected below the water to form an initially sharp, horizontal interface, within 1 to 2 millimeters of the midplane of the cell, as judged by eye. Both the water and the mixture were allowed to equilibrate at room temperature with the cell for several hours before use and were injected through 0.2 μm pore diameter cellulose acetate membrane filters. The resulting sample was nearly homogeneous in temperature, but initially contained a very strong, stabilizing concentration gradient. The resulting interfacial region was not perfectly flat, which is optically equivalent to having spurious very long wavelength fluctuations. These perturbations die away in time because of gravity, and for this reason we did not use data taken during the first 600 seconds after forming the interface.

The shadowgraph apparatus we used is shown schematically in Fig. 1. It employed a plane parallel monochromatic beam of wavelength 680 nm, having a $1/e^2$ diameter of 2.0 cm. The beam was formed by placing the 1 mW output from a single-mode optical fiber coupled directly to a superluminous diode, one focal length from an achromatic doublet of diameter 5 cm and focal length 20 cm. The beam was directed vertically downward along the axis of the sample cell after which it passed through a 5 cm diameter, 15.0 cm focal length, achromatic doublet. A JAI model CV-M10-BX,

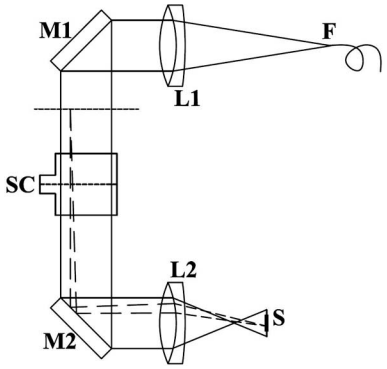

FIG. 1. Schematic diagram of the apparatus showing the sample cell (SC) and the shadowgraph arrangement. A clean diverging beam with a nearly Gaussian profile exited from the monomode fiber at F and was collimated by lens L1, with focal length 20 cm. Mirror M1 redirected the beam vertically downward, where it passed through the sample cell parallel to the concentration gradient. A second mirror, M2, together with lens L2, of focal length 15 cm, imaged the intensity distribution in the desired visualization plane onto the CCD sensor S.

8-bit CCD camera, with 8.3 μm square pixels, was placed with its sensor approximately 21 cm from the lens. It was possible to move this lens and the camera as a unit to vary the distance between them and the sample cell. No additional lens was used with the camera.

To determine the relationship between lateral distance in the sample and on the sensor, we placed a pair of Vernier calipers open to 1.00 cm in the plane that is imaged onto the sensor by the second lens. (To do this we removed the sample cell and moved the lens/camera block away from the first lens and fiber.) We then determined the size of the image (in pixels) corresponding to the opening of the caliper jaws. As a result of this calibration we determined that the central 512×512 pixel area of the sensor, which was used for the data images, corresponded to side length $W=1.132$ cm. The side length fixed the minimum q value that could be resolved at $q_{\min}=2\pi/W=5.55$ cm^{-1}. The maximum possible q that could be measured is theoretically $256\sqrt{2}q_{\min}\approx2000$ cm^{-1}, based on the number of pixels used. In practice, we could not obtain meaningful data for wave vectors above ~500 cm^{-1}, because of the effects of photon shot noise and electronic camera noise.

This optical arrangement is a bit unusual for a shadowgraph, in that the plane imaged upon the sensor actually lay on the entrance side of the sample rather than the exit side as is customary, but this still resulted in excellent shadowgraph signals (we will refer to this situation as having a negative visualization distance). As an experimental check, we took data using two different values for the visualization distance $z_o\cong-48$ and -36 cm obtained by moving the lens/camera unit so that the lens was either 5 or 17 cm beyond the center of the sample, respectively. The results did not depend on the visualization distance, except through the z-dependent shadowgraph transfer function [44], as expected.

The effect of fluctuations on the transmitted beam is to introduce time-dependent spatial modulation of the optical phase of the emerging wave because of the coupling between refractive index and concentration. As the beam propagates beyond the cell, the phase modulation develops into an intensity modulation, which can be digitized by the camera. Each image was Fourier transformed spatially to separate the contribution from fluctuations of different wave vectors. This analysis method is justified by the physical optics theory of the shadowgraph as applied to weak fluctuations [44]. The intensity variations are the result of interference between the transmitted beam and the electric field diffracted by the fluctuations, and are proportional to the diffracted electric field amplitude, rather than to its intensity.

The shadowgraph method has been used previously to measure the mean-squared amplitude of fluctuations $S(q)$, for a single-component fluid (high-pressure gas) below the onset of convection [45], and for mixtures undergoing free diffusion [36–38]. It has also been used to determine the static power spectrum of concentration fluctuations induced by a linear concentration profile generated by the Soret effect in suspensions of nanoparticles and polymer solutions [46]. In addition, both $S(q)$ and the temporal correlation function of the fluctuations present in free diffusion have been measured using either the shadowgraph [47] or a closely related Schlieren method [48,49]. These methods can provide the same information usually obtained by static and/or dynamic light scattering, provided the system under study scatters strongly enough. They have several experimental advantages relative to small angle light scattering. First, they can access wave vectors as small as a few cm^{-1}, which correspond to scattering angles of order millidegrees. Thus, they are well suited for the study of very large length scale processes. Second, they do not require accurate alignment; the angle at which light is diffracted relative to the beam determines the wave-vector component produced by interference with the beam. (Of course, any Schlieren method does require excellent control of the mask.) Third, they are relatively immune to the effects of stray elastically scattered light, provided only that the electric field of such light is small compared to that of the *beam*. Fourth, rather good statistics can be obtained in relatively short times. The reason for this is that these methods provide simultaneous measurements for many different wave vectors. The wave vectors range in magnitude from $q_{\min}=2\pi/W$, where W is the side length of the area mapped onto the sensor (assumed square), to a maximum of $Mq_{\min}/\sqrt{2}$. Here M is the number of pixels corresponding to the distance W. The number of independent wave vectors having magnitude q is roughly equal to $\pi q/q_{\min}$, and for azimuthally symmetric samples, the results (dynamic or static) for all wave vectors having the same q can be averaged. This is not a significant advantage for $q=q_{\min}$, for which only two independent measurements are obtained, but for higher q values, the advantage can be very significant.

The primary disadvantage of the shadowgraph method is the presence of the shadowgraph transfer function which, under ideal conditions, is given by [44], $T(q)=\sin^2[q^2z_o/(2k_o)]$, where z_o is the visualization distance, and k_o is the vacuum wave vector of the light. The transfer function can be made q independent by using the Schlieren method [48,49]; however, this requires maintaining ex-

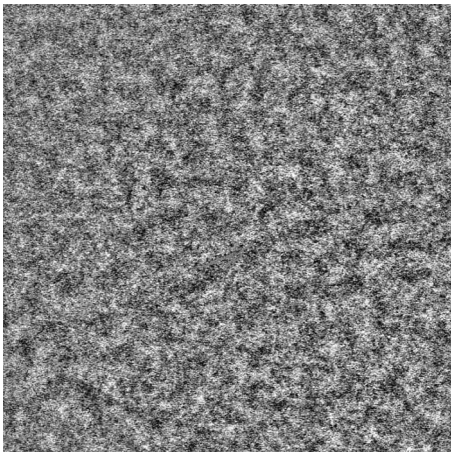

FIG. 2. Scaled difference of two shadowgraph images taken at $t \cong 600$ s, using a nominal visualization distance of −48 cm. The fluctuations are visible as the lighter and darker patches. The actual amplitude of the intensity variations was about ±4 gray levels, and the image has been gray scaled so that ±5 gray levels cover the range from black to white.

tremely precise optical alignment. The shadowgraph transfer function is observed only for sufficiently small wave vectors, where a fluctuation of a given wave vector diffracts light equally into positive and negative orders that are in phase (the Raman-Nath regime). For sufficiently high q, there is a crossover to the Bragg regime, where the fields diffracted into positive and negative orders are not correlated. A similar technique, which the authors refer to as "near field scattering" has been used in the Bragg regime, to study fluctuations [48,50–53]. All the results presented in this paper are in the Raman-Nath regime, however.

In order to measure the temporal properties of the fluctuations, we took sets of N images, separated in time by a fixed interval, $\delta t = 0.22$ s, chosen to result in significant correlation between successive images. We used values of N in the range $200 < N < 1000$. Such sets were taken beginning 10 minutes after establishing the gradient and for various times up to 43.5 hours afterward. Each image was scaled by dividing it by its own spatially averaged value to form a series of scaled images $i(\vec{x}, n\delta t)$. Here $\vec{x}$ refers to lateral position in the sample. The scaled images within one set were averaged to form a background image corresponding to the intensity profile of the beam, $i_o(\vec{x})$, which was subtracted from each scaled image in that set. A typical example of such a difference image is shown in Fig. 2. Roughly speaking, the light and dark patches correspond to regions of larger and smaller values for the vertically averaged refractive index.

We next Fourier transformed the difference images spatially to obtain a sequence of q-space "images" $i(\vec{q}, n\delta t)$ from which we calculated two quantities that we shall refer to as the measured structure factor

$$S_m(\vec{q}) = \langle |i(\vec{q}, n\delta t)|^2 \rangle_n, \tag{1}$$

and the measured correlation function,

$$G_m(\vec{q}, p\delta t) = \mathrm{Re}\{\langle i(\vec{q}, n\delta t) i^*[\vec{q}, (n+p)\delta t] \rangle_n\}. \tag{2}$$

Due to the shadowgraph transfer function, and because each image contains additive noise, uncorrelated with the fluctuations, the measured structure factor is related to that of the concentration fluctuations $S(\vec{q})$ by

$$S_m(\vec{q}) = AT(\vec{q})S(\vec{q}) + B_m(\vec{q}). \tag{3}$$

Here A is a constant relating the concentration and intensity fluctuations, $B_m(\vec{q})$ is a measurable noise background, due almost entirely to electronic and shot noise in the camera, and $T(q)$ is the shadowgraph transfer function [44]. In writing Eq. (3), we have neglected any correlation between the fluctuations and the noise. We have also observed that the noise is not correlated from image to image within our ability to measure it. Thus, *except for a time delay of zero*, the measured correlation function $G_m(\vec{q}, \tau)$ is directly proportional to the *normalized* correlation function for the concentration fluctuations $G(\vec{q}, \tau)$,

$$G_m(q, \tau) = \begin{cases} AT(q)S(q)G(q, \tau) & (\tau \neq 0), \\ S_m(q) & (\tau = 0). \end{cases} \tag{4}$$

Because of the azimuthal symmetry of the system, all measured quantities are dependent only upon the magnitude of $\vec{q}$, and thus we averaged the data azimuthally. Because $T(q)$ is not time dependent, its only effect on the dynamics is to change the amplitude of the signal. This effect was particularly noticeable near the zeroes of the transfer function, where the signals were very weak; however, if necessary, this problem can be eliminated using a Schlieren method with basically the same apparatus [48,49]. We normalized our results for $G_m(q, \tau)$ by dividing by $AT(q)S(q) = S_m(q) - B_m(q)$, to obtain experimental results for the normalized correlation function $G(q, \tau)$ $(\tau \neq 0)$.

We should point out that the local intensity fluctuations are proportional to the local beam intensity [44]; however, we did not divide by the beam profile $i_o(\vec{x})$, but instead subtracted $i_o(\vec{x})$ from each normalized image. Because of this, and because our data are limited to a measurement aperture of size $W \times W$, the result, after spatial Fourier transformation, is a convolution of the desired data with the Fourier transform of the product of the beam profile and the measurement aperture. Both of these functions are sufficiently broad in real space, so that the transform of their product is narrow enough that it did not significantly affect our results.

We obtained $S_m(\vec{q})$ by using the normalized images $i(\vec{q}, n\delta t)$ in each sequence to compute it directly. We also measured $B_m(\vec{q})$ for both visualization distances after the diffusion process was essentially complete (at 70 hours for $z_o = -47$ cm, and at 144 hours for $z_o = -36$ cm), and subtracted the result from the data for $S_m(\vec{q})$ to obtain $AS(\vec{q})T(q)$. The noise background $B_m(\vec{q})$, was measured in exactly the same manner as was $S_m(\vec{q})$. We used Eq. (4) to obtain data for the normalized correlation function $G(\vec{q}, \tau)$, for $\tau \neq 0$ from the results for $G_m(\vec{q}, \tau)$. As a further experimental check, we determined z_o from the position of the zeroes in $T(q)$ and found values of −47 and −36 cm, in good agreement with the results (−48 and −36 cm) obtained using geometrical optics.

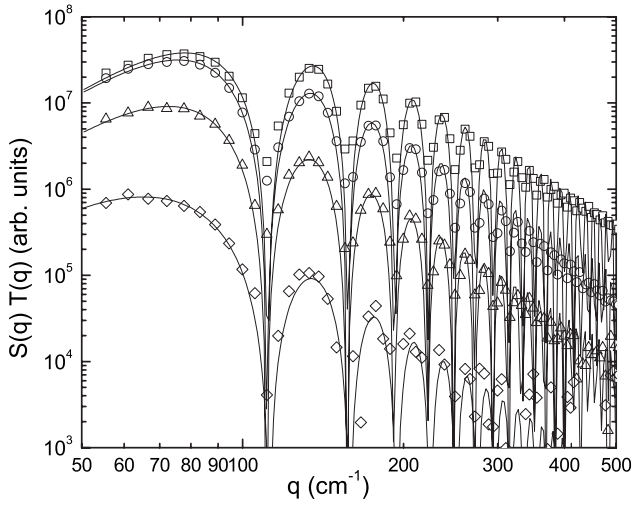

FIG. 3. Log-log graph of data for $S(q)T(q)$ taken at 600 (squares), 20 760 (circles), 72 000 (triangles), and 156 600 (diamonds) seconds after establishing the gradient. The solid curves are the result of fitting a simple function to the data (see text) to extract values for the crossover wave vector $\bar{q}_C$. The effect of the shadowgraph transfer function is evident for both the data and the fits. As can be seen, there is relatively little change in the data between $t=600$ s and $t=20\,760$ s, i.e., before the diffusing zone reaches the boundaries. However, once the concentration at the boundaries begins to change, at about 25 000 s, the signal amplitude falls dramatically.

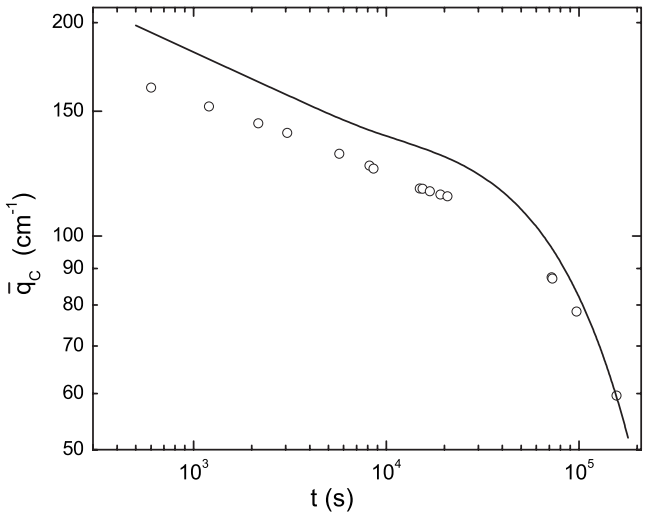

FIG. 4. The crossover wave vector $\bar{q}_C$ vs time, deduced by fitting static data of the type shown in Fig. 3. The solid curve is the result of vertically averaging the theoretical result for $S(q)$ to obtain theoretical values for $\bar{q}_C$. As can be seen, the data are not consistent with the theory. Because $\bar{q}_C$ varies only weakly with the gradient and fluid properties, we believe this discrepancy is significant.

The reader should note that the experimental transfer function of a shadowgraph apparatus inevitably deviates from the ideal form because of effects such as finite imaging region, finite sized pixels, optical aberrations, etc. In the absence of a direct calibration to determine $T(q)$, this affects the ability to measure $S(q)$, but has no effect on measurements of the shape of the correlation function. Of course, it does change the signal amplitude; however, in normalizing the measured correlation function to obtain $G(\vec{q},\tau)$, $T(q)$ cancels.

III. RESULTS AND ANALYSIS

A. Static properties

A total of 16 data runs were taken, beginning 600 s after forming the gradient, and continuing to 156 660 s later. We begin with a presentation of the results for $S(q)$ obtained from the data using Eq. (3), and the measured background levels. Figure 3 is a log-log plot of our results for $S(q)T(q)$ obtained for the runs taken at $t=600$, 20 760, 72 000, and 156 660 s (all for $z_o=-48$ cm). During a long initial period, the sample contained a decreasingly sharp gradient extending over an increasing distance on either side of the initial interface position, as the initially sharp interface broadened *via* diffusion. During this initial period, the concentration near the horizontal boundaries does not change significantly with time. Until the concentrations at the boundaries begin to change, the vertical average of the structure factor, which is what we measured, is predicted [25] to be time independent for $q \ll q_C$ but to crossover to q^{-4} behavior at a steadily decreasing wave vector, $\bar{q}_C$, which should vary roughly as $t^{-1/8}$. Once the diffusing layer reaches the boundaries, at about 25 000 s in our case, and the boundary concentrations begin changing, $S(q)$ is predicted to begin decreasing at all q, and in addition, $\bar{q}_C$ is predicted to begin falling more rapidly with time.

As may be seen, there has been only a relatively small decrease in the amplitude of the first peak near $q=80$ cm^{-1} by $t=20\,760$ s, but it begins decreasing rapidly after that.

In order to provide a more quantitative analysis, we fit the function $S(q)T(q)=S_O T(q)/[1+(q/\bar{q}_C)^4]$ to our data, adjusting z_o, S_O, and $\bar{q}_C$ for each data run, and using the ideal form for $T(q)$. The results of these fits are shown as the continuous curves in Fig. 3. All runs were consistent with $z_o=-47$ and -36 cm, which agree quite well with the values we calculated using geometrical optics. The results obtained for the effective crossover wave vector $\bar{q}_C$ were not sensitive to the data at higher q, and we are confident this is a robust parameter. We should point out, however, that use of the ideal form for $T(q)$ in fitting will result in values for $\bar{q}_C$ that are systematically small to some extent, because actual transfer functions inevitably fall off more rapidly with increasing q than does the ideal form.

We may compare the results deduced experimentally for $\bar{q}_C$ with what would be predicted for our system, using its known, concentration-dependent, fluid properties [$\beta=0.2246+0.1c-0.125c^2$, $\nu=0.01\exp(2.06c+2.32c^2)$ cm^2/s, where c is the weight fraction of glycerol, and $D=0.93\times10^{-5}$ cm^2/s] [54], and this is done in Fig. 4. The solid curve was obtained by numerically integrating Eq. (26) of Ref. [25] over the vertical extent of the sample to find a z-averaged $S(q)$, and obtaining the value of q for which the result was one-half of the $q\to0$ limit. (The results for $\bar{q}_C$

obtained in this relatively simple manner were practically identical to those obtained by fitting calculated "data" points in the same way the data were analyzed.) In carrying out the integration, we calculated the local concentration and its gradient using the value of the mass diffusion coefficient at the mean concentration of 19.5 wt. %, because the diffusion coefficient varies little with concentration over the range of our experiment (0–39 wt. %). We made the calculation both using average values for ν and β, and including their variation with concentration, but found very little difference between the two results. The effect of averaging over vertical position was larger, reducing $\bar{q}_C$ by about 10% over most of the range. The comparison between theory and experiment presented in Fig. 4, does not involve any adjustable parameters, and the discrepancy, which ranges from a few percent up to nearly 20% at the earliest time, must be regarded as real. In fact, q_C varies as only the $\frac{1}{4}$ power of the gradient and the fluid properties, so it would require a considerable error (of order 60% or more) in the gradient and/or the fluid properties to account for the difference. We think it is more likely that the theoretical treatment will have to be refined if it is to provide a more accurate description of the fluctuations present during free diffusion.

B. Dynamic properties

We turn now to a discussion of the results for the dynamic properties of the fluctuations as characterized by the normalized temporal correlation function $G(q,\tau)$, which we obtained from our measurements using Eqs. (3) and (4). Under the appropriate conditions, theory predicts [25] that the nonequilibrium portion of the spectrum of the concentration fluctuations, at height z in the sample, $S(z,q,\omega)$ is approximately Lorentzian and is given by

$$S(z,q,\omega) \cong \frac{E|\nabla c(z)|^2}{1+[q_C(z)/q]^4}\left(\frac{\Gamma(z)}{\omega^2+\Gamma(z)^2}\right), \tag{5}$$

where E is a constant, and the linewidth $\Gamma(z)$ is given by $\Gamma(z)=Dq^2\{1+[q_C(z)/q]^4\}$, with $q_C(z)=\{\beta(z)g\nabla c(z)/[\nu(z)D]\}^{1/4}$. The equilibrium portion of the signal is negligibly small for our conditions, and if one assumes the fluctuations are uncorrelated in the z direction [25], the vertical average of Eq. (5) may be compared to our data. It should be noted that the vertical averaging process results in a spectral shape that can be strongly non-Lorentzian, as discussed below.

We should point out that the result given by Eq. (5) was obtained assuming $D/\nu \ll 1$, and $4\beta g\nabla c(z,t)/(\nu^2 q^4) \ll 1$. Although the first approximation holds accurately for our system at all times, the second fails for sufficiently small q values in the region of maximum gradient. The q value for which $4\beta g\nabla c(z,t)/(\nu^2 q^4)$ exceeds 0.1 in the region of maximal gradient decreases with time, as the gradient relaxes. For example, for $t=600$ s, it exceeds 0.1 in that region for q values below 90 cm^{-1}, while for our last data set taken at $t=156\,660$ s it exceeds 0.1 only for $q<42$ cm^{-1}. Despite this, we find that the exact and approximate spectra [Eqs. (21) and (25) of [25], respectively] averaged over the vertical extent of the sample (with ν and β concentration dependent) are very similar in shape and differ by less than 5% in linewidth for rather smaller q values than those stated above. For example, the effective linewidths (half-width at half-height) agree to within 5% for q values above 55 cm^{-1} and 36 cm^{-1} for $t=600$ s and 156 660 s, respectively. Consequently, we report data for those q values and times for which the vertical average of the approximate and exact linewidths agree to within 5%, even though $4\beta g\nabla c(z,t)/(\nu^2 q^4)$ exceeds 0.1 for some of these data. Unlike the results of averaging the amplitude of the fluctuations, the effective linewidths obtained for the averaged spectra were significantly different when ν and β were taken as concentration dependent.

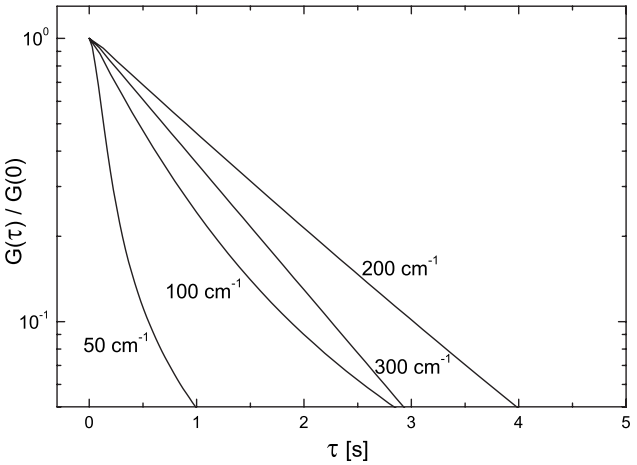

FIG. 5. Predicted correlation functions for four wave vectors as calculated for $t=600$ s. The correlation functions were calculated by vertically averaging the theoretical result for $S(q,\omega)$ and Fourier transforming with respect to ω to obtain $G(\tau)$. One can see immediately that the theory predicts a smaller decay rate for $q=200$ cm^{-1} than it does for any of the other wave vectors, i.e., the predicted behavior is strongly nondiffusive. One should also note that the theory predicts nonexponential decay at the lower wave vectors.

As mentioned above, the vertically averaged spectra depart strongly from a Lorentzian shape under some conditions (lower q and earlier times). In order to relate these theoretical results to the data for the measured correlation functions, we Fourier transformed the calculated spectra numerically to obtain corresponding theoretical correlation functions. Examples of such theoretical correlation functions are shown in Fig. 5 for several different q values as calculated for $t=600$ s. The plot is semilogarithmic, and thus exponential decay results in a straight line. Inspection reveals that the decay is predicted to be significantly nonexponential for the lowest wave vector, and that the decay rate (slope) is predicted to be greater for wave vectors both above and below the intermediate value of 200 cm^{-1}.

Figure 6 shows representative experimental results for $t=600$ s for $G(\tau)$ for the same wave vectors for which the theoretical results are shown in Fig. 5. The data reveal the predicted nonexponential decay for $q=50$ cm^{-1}, as well as the predicted nondiffusive dependence of the decay rate on the wave vector. The data presented in Fig. 6 all correspond

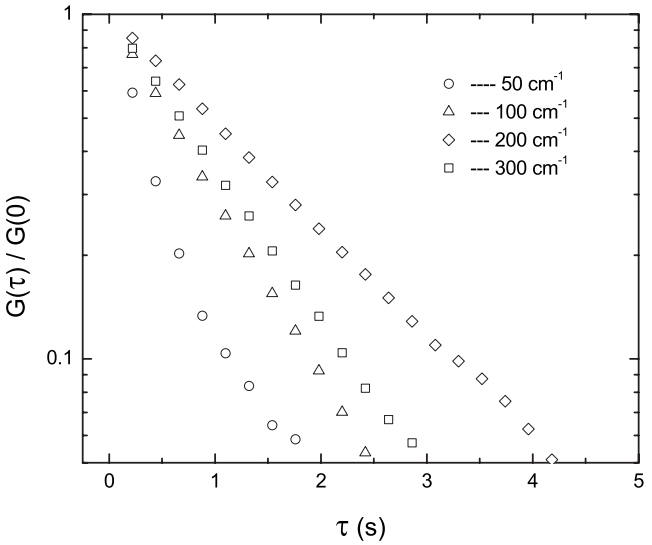

FIG. 6. Measured correlation functions for the same wave vectors as Fig. 5, obtained for $t=600$ s. We observe the predicted nondiffusive behavior, and we observe curvature for the lowest wave vector, much like that shown in Fig. 5. The slight curvature predicted for $q=100$ cm^{-1} was not within our ability to detect.

to a visualization distance of −48 cm, but the results obtained for $G(\tau)$ with $z_o=-36$ cm were indistinguishable in terms of behavior and the quality of the fits.

To provide a more global comparison of theory and experiment we determined decay rates from calculated correlation functions, such as those shown in Fig. 5. As noted, the calculated correlation functions are definitely not exponential for the smaller q values, as they would be for a Lorentzian spectrum, but become accurately exponential for sufficiently large q. Rather than attempt to characterize such complicated functions by any *ad hoc* fitting procedure for comparison with the data, we instead determined an effective decay rate as being the inverse of the delay time for which $G(\tau)$ had decayed to e^{-1} of its initial value.

Figure 7 shows the predicted and experimental results for the decay rate $\Gamma(q)$, as a function of q for runs at $t=14\,880$ s ($z_o=-48$ cm) and $t=15\,420$ s ($z_o=-36$ cm) which were made close enough together in time to be considered "simultaneous." As can be seen, the prediction that the decay rate should reach a minimum near q_C, is correct. Defining $\bar{q}_C$ to be the value for which the data reach a minimum (see the discussion preceding Fig. 9), we found values of $\bar{q}_C=126.2$ and 124.6 cm^{-1} for $t=14\,880$ and 15 420 s, respectively. The solid line is the theoretical result for the decay rate. It was obtained by finding the $1/e$ time for the Fourier transform of the vertical average of Eq. (25) of [25] using the gradient calculated at the mean time of the two runs, 15 150 s, including the concentration dependence of both β and ν. It should be noted that this result was obtained without adjustment of any parameters.

Figure 8 shows similar results, both experimental and theoretical (solid curves) for $t=600$, 3200, 19 000, and 72 000 s. As can be seen the agreement with theory becomes progressively better with increasing time, i.e., as the gradient becomes less sharp. In all cases, the predicted nondiffusive behavior is evident, and the predicted and observed wave vectors for the minimum decay rate agree reasonably well.

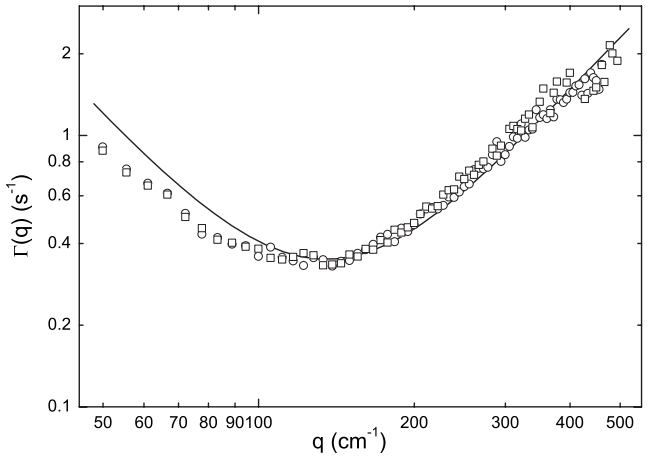

FIG. 7. The decay rate $\Gamma(q)$ vs q for data taken at $t=14\,880$ s [$z_o=-48$ cm (squares)] and $t=15\,420$ s [$z_o=-36$ cm (circles)]. As can be seen, the decay rate reaches a minimum near q_C ($\bar{q}_C=126.2$ and 124.6 cm^{-1} for $t=14\,880$ and 15 420 s, respectively). The solid line is the theoretical result, obtained as discussed in the text, including the concentration dependence of both β and ν.

In order to provide a more general comparison with theory, we calculated $\bar{q}_C$ for the dynamic properties as being the value of q for which the theoretical decay rate reached its minimum value vs q for each time. We found values for $\bar{q}_C$ by fitting the equation $\Gamma=Dq^2[1+(\bar{q}_C/q)^4]$ to the data, adjusting D and $\bar{q}_C$. Figure 9 shows results for this dynamic $\bar{q}_C$ as a function of time, both for the vertically averaged theory, using concentration-dependent fluid properties (solid line), and for comparison, the results obtained by fitting the data, as described above. The behavior is qualitatively similar to that found for the static properties (see Fig. 4), with the data

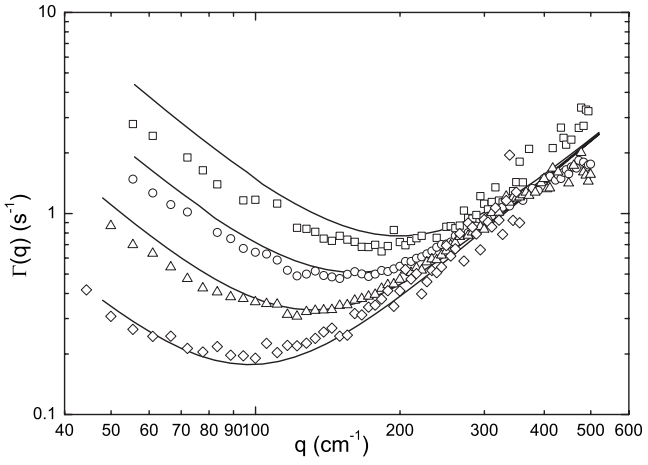

FIG. 8. Experimental (symbols) and theoretical (solid curves) results for $\Gamma(q)$ vs q for data taken at $t=600$ (squares), 3200 (circles), 19 000 (triangles), and 72 000 (diamonds) seconds. The theoretical results were obtained by vertical averaging, using concentration-dependent fluid properties, as described in the text.

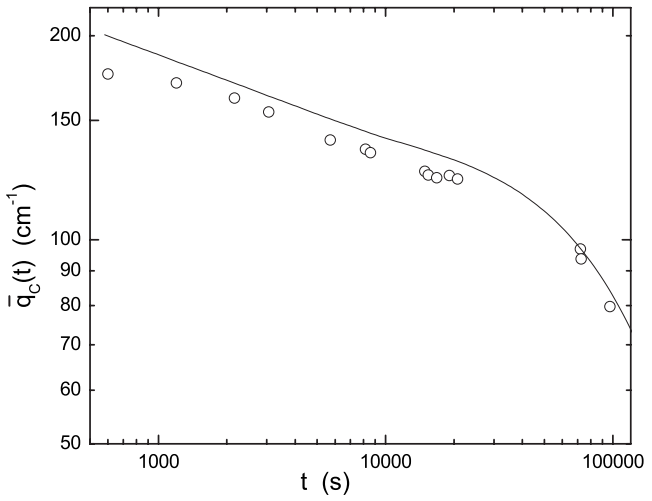

FIG. 9. An effective dynamic cutoff wave vector equal to the wave vector of minimal decay rate vs time for both data and theory.

lying below the theory, but in this case the disagreement is less. Because the results for $\bar{q}_C$ obtained from the dynamics are not affected by the transfer function, the comparison with theory should be more exact in this case. We also note that although the experimental values for $\bar{q}_C$ are somewhat dependent on whether static or dynamic properties are used to obtain them, there is no reason to expect them to be identical, once vertical averaging is involved.

In fitting the data for the decay rate, to determine $\bar{q}_C$, we also obtained values for the diffusion coefficient. The resulting values for D, over the time range 600–97 800 s, have a standard deviation of 8%, and an average value of $D=1.03 \times 10^{-5}$ cm^2/s. This result is 11% above the literature value, certainly well within what one would expect considering the vertical averaging, theoretical approximations, etc.

IV. DISCUSSION

Using a dynamic shadowgraph method, we have measured the autocorrelation function of concentration fluctuations present during free diffusion of a 39 wt. % glycerol/water solution into pure water. We find that the dynamics of concentration fluctuations present during free diffusion are strongly nondiffusive, i.e., the decay rate does not decrease monotonically with decreasing wave vector. Instead, a well-defined minimum in the decay rate of the correlation function vs wave vector is observed at all times after forming the initial gradient. This effect is predicted theoretically, and we have used vertical averaging with concentration-dependent fluid properties to compare theory and experiment, without using adjustable parameters. The agreement is reasonably good, being within about 20% or better. Given the rather weak dependence of the crossover wave vector on fluid properties, we think the discrepancy with theory is primarily the result of assumptions made in the calculations, rather than experimental errors.

ACKNOWLEDGMENTS

This work was supported by the ESA and by NASA under Grant No. NNCO4CGA45G.

[1] A. Onuki, J. Stat. Phys. **18**, 475 (1978).
[2] I. Procaccia, D. Ronis, and I. Oppenheim, Phys. Rev. Lett. **42**, 287 (1979).
[3] T. R. Kirkpatrick, and E. G. D. Cohen, Phys. Lett. **78A**, 350 (1980).
[4] A. Tremblay, E. D. Siggia, and M. Arai, Phys. Lett. **76A**, 57 (1980).
[5] A. M. S. Tremblay, M. Arai, and E. D. Siggia, Phys. Rev. A **23**, 1451 (1981).
[6] T. R. Kirkpatrick, E. G. D. Cohen, and J. R. Dorfman, Phys. Rev. A **26**, 950 (1982).
[7] T. R. Kirkpatrick, E. G. D. Cohen, and J. R. Dorfman, Phys. Rev. A **26**, 972 (1982).
[8] T. R. Kirkpatrick, E. G. D. Cohen, and J. R. Dorfman, Phys. Rev. A **26**, 995 (1982).
[9] D. Ronis and I. Procaccia, Phys. Rev. A **26**, 1812 (1982).
[10] T. R. Kirkpatrick and E. G. D. Cohen, J. Stat. Phys. **33**, 639 (1983).
[11] R. Schmitz and E. G. D. Cohen, J. Stat. Phys. **38**, 285 (1985).
[12] R. Schmitz and E. G. D. Cohen, J. Stat. Phys. **40**, 431 (1985).
[13] B. M. Law, R. W. Gammon, and J. V. Sengers, Phys. Rev. Lett. **60**, 1554 (1988).
[14] B. M. Law and J. V. Sengers, J. Stat. Phys. **57**, 531 (1989).
[15] B. M. Law, P. N. Segrè, R. W. Gammon, and J. V. Sengers, Phys. Rev. A **41**, 816 (1990).
[16] P. N. Segrè, R. W. Gammon, J. V. Sengers, and B. M. Law, Phys. Rev. A **45**, 714 (1992).
[17] P. N. Segrè, R. Schmitz, and J. V. Sengers, Physica A **195**, 31 (1993).
[18] J. M. Ortiz de Zárate, R. P. Cordón, and J. V. Sengers, Physica A **291**, 113 (2001).
[19] J. M. Ortiz de Zárate and L. Muñoz Redondo, Eur. Phys. J. B **21**, 135 (2001).
[20] J. M. Ortiz de Zárate and J. V. Sengers, Physica A **300**, 25 (2001).
[21] J. M. Ortiz de Zárate and J. V. Sengers, Phys. Rev. E **66**, 036305 (2002).
[22] L. D. Landau and E. M. Lifshitz, *Fluid Mechanics* (Pergamon, New York, 1959).
[23] J. M. Ortiz de Zárate, F. Peluso, and J. V. Sengers, Eur. Phys. J. E **15**, 319 (2004).
[24] P. N. Segrè and J. V. Sengers, Physica A **198**, 46 (1993).
[25] A. Vailati and M. Giglio, Phys. Rev. E **58**, 4361 (1998).
[26] D. Brogioli and A. Vailati, Phys. Rev. E **63**, 012105 (2000).
[27] J. V. Sengers and J. M. Ortiz de Zárate, Rev. Mex. Fis. **48**, Suppl. 1, 14 (2002).
[28] J. M. Ortiz de Zárate, J. A. Fornés, and J. V. Sengers, Phys. Rev. E **74**, 046305 (2006).
[29] J. M. Ortiz de Zárate and J. V. Sengers, *Hydrodynamic Fluctuations* (Elsevier, Oxford, Great Britain, 2006).

[30] W. B. Li, P. N. Segrè, R. W. Gammon, and J. V. Sengers, Physica A **204**, 399 (1994).
[31] P. N. Segrè, R. W. Gammon, and J. V. Sengers, Phys. Rev. E **47**, 1026 (1993).
[32] A. Vailati and M. Giglio, Phys. Rev. Lett. **77**, 1484 (1996).
[33] A. Vailati and M. Giglio, Prog. Colloid Polym. Sci. **104**, 76 (1997).
[34] A. Vailati and M. Giglio, Physica A **235**, 105 (1997).
[35] W. B. Li, K. J. Zhang, J. V. Sengers, R. W. Gammon, and J. M. Ortiz de Zárate, Phys. Rev. Lett. **81**, 5580 (1998).
[36] A. Vailati and M. Giglio, Nature (London) **390**, 262 (1997).
[37] D. Brogioli, A. Vailati, and M. Giglio, Phys. Rev. E **61**, R1 (2000).
[38] D. Brogioli, A. Vailati, and M. Giglio, J. Phys.: Condens. Matter **12**, A39 (2000).
[39] P. Cicuta, A. Vailati, and M. Giglio, Phys. Rev. E **62**, 4920 (2000).
[40] P. Cicuta, A. Vailati, and M. Giglio, Appl. Opt. **40**, 4140 (2001).
[41] G. Z. Gershuni and E. M. Zhukhovitskii, *Convective Stability of Incompressible Fluids* (Keter Publishing House, Jerusalem, 1976).
[42] J. P. Boon, C. Allain, and P. Lallemand, Phys. Rev. Lett. **43**, 199 (1979).
[43] J. Oh, J. M. Ortiz de Zárate, J. V. Sengers, and G. Ahlers, Phys. Rev. E **69**, 021106 (2004).
[44] S. P. Trainoff and D. S. Cannell, Phys. Fluids **14**, 1340 (2002).
[45] M. Wu, G. Ahlers, and D. S. Cannell, Phys. Rev. Lett. **75**, 1743 (1995).
[46] A. Vailati *et al.*, Appl. Opt. **45**, 2155 (2006).
[47] F. Croccolo, D. Brogioli, A. Vailati, M. Giglio, and D. S. Cannell, Ann. N.Y. Acad. Sci. **10**, 365 (2006).
[48] D. Brogioli, A. Vailati, and M. Giglio, Europhys. Lett. **63**, 220 (2003).
[49] F. Croccolo, D. Brogioli, A. Vailati, M. Giglio, and D. S. Cannell, Appl. Opt. **45**, 2166 (2006).
[50] M. Giglio, M. Carpineti, and A. Vailati, Phys. Rev. Lett. **85**, 1416 (2000).
[51] M. Giglio, M. Carpineti, A. Vailati, and D. Brogioli, Appl. Opt. **40**, 4036 (2001).
[52] D. Brogioli, A. Vailati, and M. Giglio, Appl. Phys. Lett. **81**, 4109 (2002).
[53] M. Giglio, D. Brogioli, M. A. C. Potenza, and A. Vailati, Phys. Chem. Chem. Phys. **6**, 1547 (2004).
[54] A. V. Wolf, B. G. Brown, and P. G. Prentiss, *Handbook of Chemistry and Physics*, 69th ed. (CRC, Boca Raton, FL, 1988).